Prelaunch Algorithm and Data Format for the Level 1 Calibration Products for the EOS-AM1 Moderate Resolution Imaging Spectroradiometer (MODIS)

B. Guenther, Gerald D. Godden, Xiaoxiong Xiong, Edward J. Knight, Shi-Yue Qiu, Harry Montgomery, M. M. Hopkins, Mohammad G. Khayat, and Zhidong Hao

***Abstract*—The Moderate Resolution Imaging Spectroradiometer (MODIS) radiometric calibration product (Level 1B) is described for the thermal emissive and reflective solar bands. A band-integrated radiance is produced for all measurements. A reflectance factor product is also produced for the reflected solar band measurements. Specific sensor design characteristics are identified to assist in understanding how the calibration algorithm software product is designed. The product file format is summarized, and the location for the current file format is provided.**

I. Introduction

THIS PAPER describes the Moderate Resolution Imaging Spectroradiometer (MODIS) calibration data product. The calibration equations for this product are developed, and the approaches for the laboratory calibration and the on-orbit verification of that calibration are described. The development of the MODIS science products begins with the Level 1B calibration products. The radiometric characteristics of the L1B product are reviewed here, but the geometric registration and spectral characterization of the products are not described. The primary aspects of the MODIS sensor is discussed by Barnes *et al.* [1]. Major science products for the MODIS oceans [2] and land surface [3] research communities are described elsewhere in this issue.

Sensor design and characteristics necessary to understand the Level 1B software product are reviewed in Section II. The emissive infrared algorithms are described in Section III. The reflected solar bands algorithm, including subsections on the radiance and the reflectance factor products, is covered in Section IV. The Level 1B data software product attributes, such as file format and uncertainty index, are reviewed in Section V. The conclusion and summary comments are provided in Section VI.

Manuscript received November 5, 1997; revised April 17, 1998.

B. Guenther and H. Montgomery are with NASA's Goddard Space Flight Center, Greenbelt, MD 20771 USA (e-mail: guenther@ltpmail.gsfc.nasa.gov).

G. D. Godden is with Physics Application, Inc., Vienna, VA 22182 USA.

X. Xiong is with Science Systems and Applications, Inc., Lanham, MD 20706 USA.

E. J. Knight and M. G. Khayat are with Research and Data Systems Corporation, Greenbelt, MD 20770 USA.

S.-Y. Qiu is with Computation Physics Applications, Inc., Columbia, MD 21042 USA.

M. M. Hopkins and Z. Hao are with General Sciences Corporation, Laurel, MD 20707 USA.

Publisher Item Identifier S 0196-2892(98)04894-3.

The calibration and test data analysis for the MODIS Science Team is performed by the MODIS Characterization Support Team (MCST). MCST also has developed the MODIS Level 1B calibration algorithm. All authors of this paper have been or are currently members of the MCST.

II. Instrument Background

The MODIS is a 36-band spectroradiometer that covers a broad spectral range and has very demanding calibration performance characteristics. The sensor design incorporates a paddle-wheel scan mirror to provide a wide swath across the earth's surface and access to an array of characterization subsystems on each rotation of the mirror. The spectral separation of the light mainly comes from three dichroics and sliver interference filters at each detector. The spectral ranges for the reflected solar bands (0.4–2.3 μm) and the emissive infrared bands (3.6–14.4 μm) are calibrated and analyzed with separate techniques. The descriptions of the calibration approach and algorithm follow this separation.

Fig. 1 provides a schematic of the sensor optics, optical detectors, and electronics to demonstrate how optical signals onto the scan mirror are transformed to digital signals or data. The characterization subsystems are called onboard calibration (OBC) targets. This figure depicts the order that the OBC's are observed within a mirror rotation as well as the location of the earth observations within that rotation. The scan mirror is double sided, and both sides are used for the MODIS observations. A rotation of 360° of the scan mirror requires 2.954 s. Throughout this paper, a period of 1.477 s is identified as a scan, and the data produced from it are called a scan line of data, or a scan line. Scan lines are acquired alternately by mirror side A (MS A) and mirror side B (MS B) in the data set.

The location of a target within a scan line can be identified by its principal scan angle. The position of each OBC, the location of the earth view around the scan, and the location of the laboratory calibration sources are shown in Fig. 2. The principal scan angle is referenced to NADIR, where it has a value of zero. Fig. 2 also indicates the angle of incidence (AOI) on the scan mirror for each of these targets.

The earth scenes are sampled 1354 times over a range of principal scan angles of -55 to $+55°$. All samples are coregistered in the sensor data system as frames and telemetered together to the ground. At the NADIR, a frame is 10 000-m

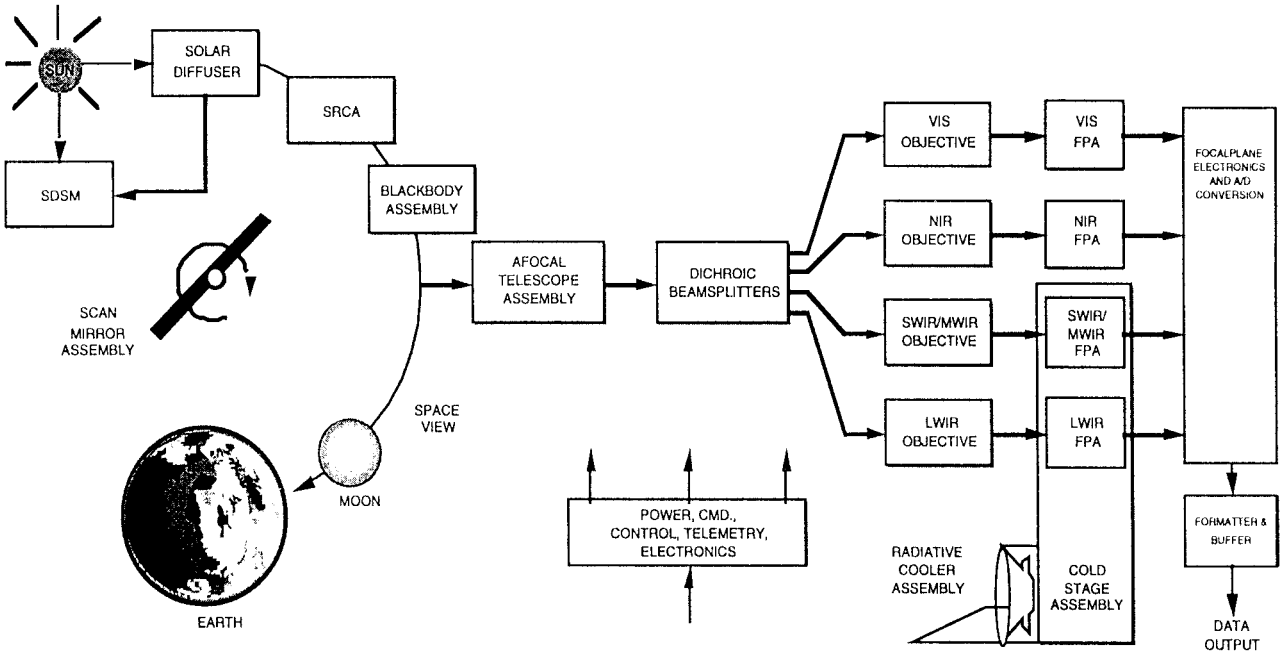

Fig. 1. Schematic of MODIS demonstrating the conversion of incident light to digital data output, the relative location of the various targets that the sensor scan mirror observes, the fundamental optics and detectors layout, and the digitizing electronics.

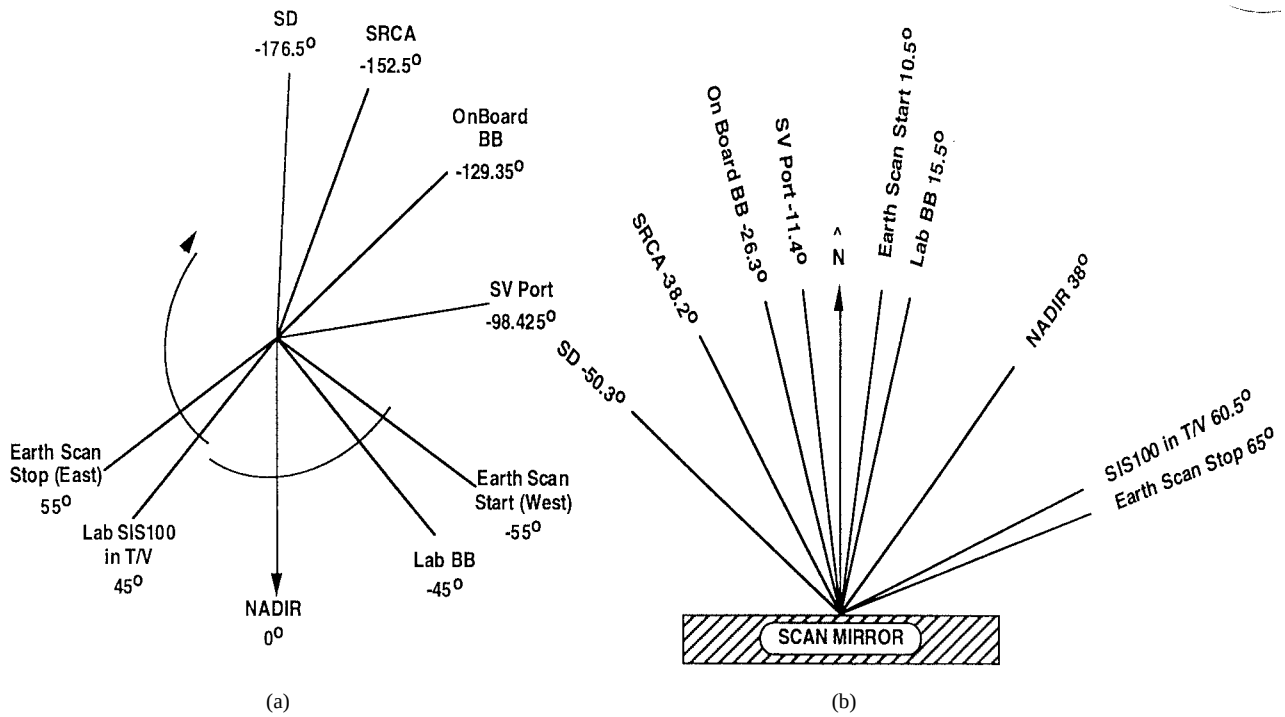

(a) (b)

Fig. 2. (a) Location in terms of the principal scan angles within a MODIS scan, of various targets, including both the in-laboratory calibration sources and the onboard sensor calibrators and the earth scenes. The principal scan angle corresponds to the degrees of rotation the mirror moves between the center location for each target, with 0° rotation selected at NADIR for the earth scene. (b) Angles of incidence (AOI) on the scan mirror within a MODIS scan of various targets is depicted.

extent in the track direction (spacecraft orbital direction) and 1000-m extent in the scan direction (orthogonal to the spacecraft direction orbital direction).

The sensor has bands with three ground resolutions of 250, 500, and 1000 m. The 1000-m bands are sampled once each frame and composed of ten channels (individual detectors) in each band. The 500-m bands are sampled twice each frame and composed of 20 channels in each band. The 250-m bands are sampled four times each frame and composed of 40 channels in each band. All detectors have a field-of-view that is approximately square. The channels are positioned end-to-end in the track direction for each band on each focal plane.

The instantaneous ground resolution of 1000, 500, and 250 m correspond to the NADIR observations. The ground resolution expands by greater than a factor of two toward the end of each scan due to the earth curvature, as viewed from the spacecraft altitude of 705 km.

The MODIS bands are positioned in four separate focal planes, with bands with center wavelengths between 0.42 and 0.55 μm on the visible (VIS) wavelength focal plane, with center wavelengths 0.64–0.94 μm on the near-infrared (NIR) wavelength focal plane, with center wavelengths 1.2–2.3 and 3.6–4.5 μm on the short-infrared and middle-infrared (SW/MWIR) wavelength focal plane and with center wavelengths 6.5–14.2 μm on the long-infrared (LWIR) wavelength focal plane. The SW/MWIR and LWIR focal planes are housed together within the MODIS radiative cooler. Information on the spectral bandpasses in the sensor specification for the MODIS are available in [1], and the definitive relative spectral responses are available through the MCST Homepage on the World Wide Web at http://ltpwww.gsfc.nasa.gov/MODIS/MCST/Home.html, under "Individual Bands Data."

The important characteristics of the OBC subsystems follow.

A. Solar Diffuser

The solar diffuser is a flat surface. The composition of the surface is Spectralon[1], and the manufacturer specifications of the reflectance of this surface [4] are presented in Fig. 3. The reflectance of this diffuser has very small variations with wavelength across all MODIS solar reflected bands, except for the variation across Band 7.

B. Spectroradiometric Calibration Assembly

The Spectroradiometric Calibration Assembly (SRCA) comprises a source assembly, monochromator, transfer optics, and collimating optics on the output. It includes internal diode detectors to track subsystem characteristics. The SRCA is used on-orbit for spectral bandpass knowledge of the reflected solar bands and within an orbit radiometric stability verification of the reflected solar bands. The radiometric sensitivity to temperature variations is determined in prelaunch thermal vacuum testing. The temperature sensitivity is verified on-orbit by tracking the response of MODIS to the SRCA through the intraorbit temperature range, when the SRCA is operated in the radiometric mode.

C. Blackbody

The Blackbody (BB) is of a V-groove design that has an emissivity of 0.993 in the direction it is used by MODIS. Twelve thermistors are distributed across the surface of the BB.

D. Space View Port

The Space View Port (SV) is an aperture in the side of MODIS that provides a view of cold space to allow for a zero radiance input signal on each scan. This zero input radiance on each scan in the emissive infrared allows a measurement of the MODIS self-radiation. The sensor operates with "warm" optics, and the optics contribute a significant amount of signal for each observation. The signal from a scene is then determined by subtracting the sensor self-radiation response on each scan.

[1] Spectralon is a trademark of Labsphere, Inc.

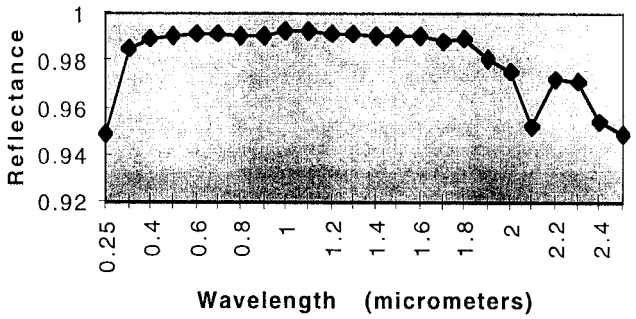

Fig. 3. Manufacturer specifications of the reflectance of a Spectralon diffuse scatter target is shown for the wavelengths between 0.25 and 2.5 μm. The MODIS bands have center wavelengths between 0.42 and 2.10 μm. The MODIS Band 7 center wavelength nearly corresponds to the dip in the reflectance of Spectralon diffuser.

III. MODIS Thermal Emissive Bands Radiometric Calibration Algorithm

We have pursued two independent calibration methodologies for the MODIS thermal bands. The first method is based on the traditional technique of fitting the instrument output digital numbers (DN's) versus radiance (L) [Watts/(m$^2 * sr * \mu$m)] distribution to a quadratic polynomial expression and is similar in form to the algorithm suggested by Young [5]. This is referred to as the L versus DN algorithm. The second method is based on a somewhat more physical approach of converting the output DN's to detector output voltages (V), incorporating the telemetered detector response to scenes onto the scan mirror with zero-radiance, and fitting these results to a second-order equation that applies a local curvature as a function of the signal level. The signal level of the detectors in the second method is due to the combination of scene radiance (on to the scan mirror) plus instrument background radiance and detector offset. This is referred to as the V versus L algorithm and is described by Knowles *et al.* [6]. This paper presents an overview of the first method, which is planned to be the baseline algorithm at launch. Investigation of the more complex (and perhaps more physical) V versus L algorithm performance, and comparison with the L versus DN algorithm, is a subject of continuing research and is not presented here. In this discussion, we do not consider the combined effects of possible scene polarization and MODIS MWIR and LWIR optical train polarization. The effects of MODIS polarization on unpolarized scenes are estimated to be small compared to specified radiance uncertainties [7]. These effects will be addressed in a subsequent publication.

The MODIS thermal emissive bands (bands 20–25 and 27–36) covering the wavelength region from 3.75 to 14.24 μm and consisting of ten channels per band are radiometrically calibrated on the ground using a precision Blackbody Calibration

Source (BCS), which is contained within the thermal vacuum chamber with the MODIS during calibration. The BCS is of the "buried-first bounce" type design and is expected to have an emissivity of 0.9995. It is located at $-45°$ scan angle, with respect to the MODIS NADIR viewing scan position in the 110° earth view scan angle range. This translates into a low AOI (15.5°) on the scan mirror to minimize reflectance variation effects. The onboard calibrator blackbody (OBC BB) and the SV are viewed once per scan mirror rotation by each side of the scan mirror. During thermal vacuum calibration, the SV is covered with a cryogenically cooled Space View Source (SVS) to simulate the on-orbit view of cold space.

The BCS emissivity is calculated, based on the design of the BCS and a measurement of the reflectance of the materials that comprise the BCS. The BSC temperature is measured with thermistors that have a temperature calibration traceable to an NIST standard temperature measurement. Consequently, the MODIS thermal emissive band calibration pedigree is based on a temperature standard, not on a radiometric standard.

The silver-coated scan mirror exhibits a significant variation in average reflectance as a function of wavelength and AOI (Cafferty [8] and MacDonald [9]) within this spectral region. In addition to the wavelength-dependent reflectivity for the scan mirror, the AOI locations of the BCS, OBC BB, and the SVS are critical factors that must be incorporated into the algorithm. The locations of these sources along a scan are depicted in Fig. 2.

The prelaunch calibration is based on the laboratory BCS. The BCS calibration is imprinted onto the OBC BB, and the on-orbit calibration is maintained with the OBC BB and SV combination.

A. Prelaunch Radiometric Calibration Algorithm

The MODIS is a conventional differencing radiometer. Instrument background radiation effects are removed by subtracting the cold space view signal from the earth view signal on a scan-by-scan basis. During thermal vacuum calibration, the spectral radiance from the BCS, after reflection from the scan mirror, is given by

$$L_{\mathrm{BCS\_PATH}} = \rho^{\mathrm{sm}}_{\mathrm{BCS}}\varepsilon_{\mathrm{BCS}}L(T_{\mathrm{BCS}}) + \left(1-\rho^{\mathrm{sm}}_{\mathrm{BCS}}\right)L(T_{\mathrm{sm}}) + L'_{\mathrm{BKG}} \quad (1)$$

where $\rho^{\mathrm{sm}}_{\mathrm{BCS}}$ is the scan mirror reflectivity integrated over the relative spectral response at the AOI for the BCS, $\varepsilon_{\mathrm{BCS}}$ represents the BCS emissivity, $L(T_{\mathrm{BCS}})$ is the radiance calculated from the Planck equation at the BCS temperature T_{BCS}, $L(T_{\mathrm{sm}})$ is the radiance calculated from the Planck equation at scan mirror temperature T_{sm}, and L'_{BKG} is the instrument background radiance exclusive of the scan mirror emission. The second term of this equation represents the emission from the scan mirror. This term is separated from the total instrument background to explicitly capture its scan angle and temperature dependence. The BCS is temperature cycled over an interval of 170–340 K.

Similarly, when the MODIS views the SVS, the spectral radiance after the scan mirror is given by

$$L_{\mathrm{SVS\_PATH}} = \left(1-\rho^{\mathrm{sm}}_{\mathrm{SVS}}\right)L(T_{\mathrm{sm}}) + L'_{\mathrm{BKG}}. \quad (2)$$

To remove the variable instrument background effect, the SVS term is subtracted from the input signal. Thus, the spectral radiance difference is

$$\Delta L_{\mathrm{BCS}} = L_{\mathrm{BCS\_PATH}} - L_{\mathrm{SVS\_PATH}} = \rho^{\mathrm{sm}}_{\mathrm{BCS}}\varepsilon_{\mathrm{BCS}}L(T_{\mathrm{BCS}}) + \left(\rho^{\mathrm{sm}}_{\mathrm{SVS}} - \rho^{\mathrm{sm}}_{\mathrm{BCS}}\right)L(T_{\mathrm{sm}}). \quad (3)$$

For a specific MODIS thermal emissive band (B), the band-averaged radiance difference, due to the BCS path and the SVS path, is

$$\Delta L_{\mathrm{BCS}}(B) = \rho^{\mathrm{sm}}_{\mathrm{BCS}}\varepsilon_{\mathrm{BCS}}\overline{L(T_{\mathrm{BCS}})} + \left(\rho^{\mathrm{sm}}_{\mathrm{SVS}} - \rho^{\mathrm{sm}}_{\mathrm{BCS}}\right)\overline{L(T_{\mathrm{sm}})} \quad (4)$$

where

$$\overline{L(T_{\mathrm{BCS}})} = \frac{\int L(T_{\mathrm{BCS}},\lambda)\mathrm{RSR}(B,\lambda)\,d\lambda}{\int \mathrm{RSR}(B,\lambda)\,d\lambda} \quad (5)$$

and $\mathrm{RSR}(B,\lambda)$ represents the wavelength-dependent relative spectral response (RSR) (normalized to unity at peak) for band B, and a similar expression for the band integration applies to the second term on the right-hand side of (4). Note that throughout this discussion, the channel number indexes are suppressed for clarity.

The band-integrated radiance difference $\Delta L_{\mathrm{BCS}}(B)$ is a function of $\mathrm{DN}_{\mathrm{BCS}} - \mathrm{DN}_{\mathrm{SVS}}$. Let

$$dn_{\mathrm{BCS}} = \frac{1}{N_{\mathrm{scans}}}\sum_{n=1}^{N_{\mathrm{scans}}}\left[\frac{1}{M_{\mathrm{BCS}}}\sum_{m=1}^{M_{\mathrm{BCS}}}\mathrm{DN}_{\mathrm{BCS}} - \frac{1}{M_{\mathrm{SVS}}}\sum_{m=1}^{M_{\mathrm{SVS}}}\mathrm{DN}_{\mathrm{SVS}}\right] \quad (6)$$

where M_{BCS} (number of BCS frames), M_{SVS} (number of SVS frames), and N_{scans} (number of scans) are appropriately smoothing intervals to optimize the calibration coefficients.

On the basis of experience with similar instruments and observed temperature dependencies, we postulate a temperature-dependent second-order nonlinear behavior for $\Delta L_{\mathrm{BCS}}(B, T_{\mathrm{instr}})$

$$\Delta L_{\mathrm{BCS}}(B,T_{\mathrm{instr}}) = a_0^{\mathrm{BCS}}(B,T_{\mathrm{instr}}) + a_1^{\mathrm{BCS}}(B,T_{\mathrm{instr}})\cdot dn_{\mathrm{BCS}} + a_2^{\mathrm{BCS}}(B,T_{\mathrm{instr}})\cdot(dn_{\mathrm{BCS}})^2 \quad (7)$$

or

$$\rho^{\mathrm{sm}}_{\mathrm{BCS}}\varepsilon_{\mathrm{BCS}}\overline{L(T_{\mathrm{BCS}})} + \left(\rho^{\mathrm{sm}}_{\mathrm{SVS}} - \rho^{\mathrm{sm}}_{\mathrm{BCS}}\right)L\overline{(T_{\mathrm{sm}})} = a_0^{\mathrm{BCS}}(B,T_{\mathrm{instr}}) + a_1^{\mathrm{BCS}}(B,T_{\mathrm{instr}})\cdot dn_{\mathrm{BCS}} + a_2^{\mathrm{BCS}}(B,T_{\mathrm{instr}})\cdot(dn_{\mathrm{BCS}})^2. \quad (8)$$

The BCS calibration coefficients $a_0^{\mathrm{BCS}}(B,T_{\mathrm{instr}})$, $a_1^{\mathrm{BCS}}(B,T_{\mathrm{instr}})$, and $a_2^{\mathrm{BCS}}(B,T_{\mathrm{instr}})$ are determined by least-squares fitting to the corresponding data. In this formulation, $a_0^{\mathrm{BCS}}(B,T_{\mathrm{instr}})$ term is viewed as part of the least-squares fitting process. It is expected to take on small nonzero values. The contribution from the nonlinear response term $a_2^{\mathrm{BCS}}(B,T_{\mathrm{instr}})$ is very small compared to the linear response term. Apart from the temperature-dependent behavior, both $a_0^{\mathrm{BCS}}(B,T_{\mathrm{instr}})$ and $a_2^{\mathrm{BCS}}(B,T_{\mathrm{instr}})$ terms will be fixed for the on-orbit operation.

B. On-Orbit Radiometric Algorithm

When the MODIS views the OBC BB, the spectral radiance after the scan mirror includes the OBC BB emitted radiance reflected by the scan mirror, the scan mirror emittance, the scan cavity emittance reflected by the OBC BB and then in turn by the scan mirror, and the remaining instrument background radiance. Thus

$$L_{\mathrm{BB\_PATH}} = \varepsilon_{\mathrm{BB}} L(T_{\mathrm{BB}})\rho_{\mathrm{BB}}^{\mathrm{sm}} + \left(1-\rho_{\mathrm{BB}}^{\mathrm{sm}}\right)L(T_{\mathrm{sm}}) + \varepsilon_{\mathrm{cav}} L(T_{\mathrm{cav}})\left(1-\varepsilon_{\mathrm{BB}}\right)\rho_{\mathrm{BB}}^{\mathrm{sm}} + L'_{\mathrm{BKG}} \quad (9)$$

where $\varepsilon_{\mathrm{BB}}$ is the OBC BB emissivity, $(1-\varepsilon_{\mathrm{BB}})$ is the reflectivity of the OBC BB, and $\varepsilon_{\mathrm{cav}}$ represents the MODIS scan cavity effective emissivity that must account for the earth and space view apertures.

From (2) and (9), the spectral radiance difference attributed to the OBC BB path and the space view path is given by

$$\begin{aligned}\Delta L_{\mathrm{BB}} &= L_{\mathrm{BB\_PATH}} - L_{\mathrm{SV\_PATH}} \\ &= \rho_{\mathrm{BB}}^{\mathrm{sm}}\varepsilon_{\mathrm{BB}}L(T_{\mathrm{BB}}) + \left(\rho_{\mathrm{SV}}^{\mathrm{sm}} - \rho_{\mathrm{BB}}^{\mathrm{sm}}\right)L(T_{\mathrm{sm}}) \\ &\quad + (1-\varepsilon_{\mathrm{BB}})\varepsilon_{\mathrm{cav}}\rho_{\mathrm{BB}}^{\mathrm{sm}}L(T_{\mathrm{cav}}). \end{aligned} \quad (10)$$

For a specific MODIS band, the band-averaged radiance difference between the OBC BB path and the space view path is given by

$$\Delta L_{\mathrm{BB}}(B) = \rho_{\mathrm{BB}}^{\mathrm{sm}}\varepsilon_{\mathrm{BB}}\overline{L(T_{\mathrm{BB}})} + \left(\rho_{\mathrm{SV}}^{\mathrm{sm}} - \rho_{\mathrm{BB}}^{\mathrm{sm}}\right)\overline{L(T_{\mathrm{sm}})} + (1-\varepsilon_{\mathrm{BB}})\varepsilon_{\mathrm{CAV}}\rho_{\mathrm{BB}}^{\mathrm{sm}}\overline{L(T_{\mathrm{CAV}})} \quad (11)$$

where $\overline{L(T_{\mathrm{BB}})}$, $\overline{L(T_{\mathrm{sm}})}$, and $\overline{L(T_{\mathrm{CAV}})}$ are the Planck emission terms determined using (5).

The earth-view sector radiance is determined using the on-orbit calibration coefficient obtained with the OBC BB and the space view and the prelaunch second-order calibration coefficients determined from the thermal vacuum BCS data sets. Equation (12) describes the use of these coefficients

$$\Delta L_{\mathrm{EV}}(B, T_{\mathrm{instr}}) = a_0^{\mathrm{BCS}}(B, T_{\mathrm{instr}}) + b_1^{\mathrm{BB}}(B, T_{\mathrm{instr}})\cdot dn_{\mathrm{EV}} + a_2^{\mathrm{BCS}}(B, T_{\mathrm{instr}})\cdot (dn_{\mathrm{EV}})^2 \quad (12)$$

where the residual offset coefficient $a_0^{\mathrm{BCS}}(B, T_{\mathrm{instr}})$ and second-order coefficient $a_2^{\mathrm{BCS}}(B, T_{\mathrm{instr}})$ are determined using (8), and the linear response $b_1^{\mathrm{BB}}(B, T_{\mathrm{instr}})$ is determined on a scan-by-scan basis by

$$b_1^{\mathrm{BB}}(B) = \frac{\Delta L_{\mathrm{BB}}(B) - a_0^{\mathrm{BCS}}(B) - a_2^{\mathrm{BCS}}(B)\cdot (dn_{\mathrm{BB}})^2}{dn_{\mathrm{BB}}} \quad (13)$$

where $\Delta L_{\mathrm{BB}}(B)$ is given by (11) and

$$dn_{\mathrm{BB}} = \frac{1}{M_{\mathrm{BB}}}\sum_{i=1}^{M_{\mathrm{BB}}} \mathrm{DN}_{\mathrm{BB}} - \frac{1}{M_{\mathrm{SVS}}}\sum_{i=1}^{M_{\mathrm{SVS}}} \mathrm{DN}_{\mathrm{SVS}}. \quad (14)$$

To achieve slowly varying behavior, the linear response term is averaged over N_{scans}

$$\overline{b_1^{\mathrm{BB}}(B)} = \frac{1}{N_{\mathrm{Scans}}}\sum_{j=-N_{\mathrm{Scans}}/2}^{N_{\mathrm{Scans}}/2} b_{1,j}^{\mathrm{BB}}(B). \quad (15)$$

The MODIS scan mirror takes 2.954 s to complete a rotation. During each scan, a new measurement of the linear response (gain) is determined according to (14). The drift of the gain from scan to scan is expected to be very small. This slowly varying behavior is considered by averaging the linear response term over N_{scans}, as shown in (15).

The OBC BB will be cycled to 315 K and allowed to return to the sensor thermal ambient temperature on an approximately biweekly basis. This OBC elevated temperature operation will simulate the ground calibration process from which the calibration coefficients were calculated. This cycle will allow for a determination of $b_1^{\text{BB-elev}}(B)$. Comparison of $b_1^{\text{BB-elev}}(B)$ with $b_1^{\mathrm{BB}}(B, T_{\mathrm{instr}})$ will verify the continued stability of on-orbit operation of a_0^{BCS} and a_2^{BCS}. Vicarious calibration measurements obtained during the validation phase of the MODIS will also be used to verify the stability on-orbit operation of a_0^{BCS} and a_2^{BCS} and the performance of the OBC BB.

There is a small time difference between when the data from the OBC BB and SV targets are collected for the gain calculation and when the earth view data are collected. During this time interval, the instrument background may be expected to drift a small relative amount due to $1/f$ noise. In a manner analogous to that suggested by Knowles *et al.* [6], a portion of this drift can be reduced by linear interpolation between successive scans.

Using the average gain (i.e., the linear response), the dn difference $\Delta_{\mathrm{BB},i}$ for a given band between the ith measurement and the average of many measurements of the OBC BB is given by:

$$\begin{aligned}\Delta_{\mathrm{BB},i} &= dn_{\mathrm{BB},i} - \overline{dn_{\mathrm{BB},i}} \\ &= dn_{\mathrm{BB},i} - \frac{\Delta L_{\mathrm{BB},i}(B) - a_2^{\mathrm{BCS}}\cdot dn_{\mathrm{BB},i}^2 - a_0^{\mathrm{BCS}}}{\overline{b_{1,i}^{\mathrm{BB}}}}. \end{aligned} \quad (16)$$

Similarly for the scan $i+1$

$$\begin{aligned}\Delta_{\mathrm{BB},i+1} &= dn_{\mathrm{BB},i+1} - \overline{dn_{\mathrm{BB},i+1}} = dn_{\mathrm{BB},i+1} \\ &\quad - \frac{\Delta L_{\mathrm{BB},i+1}(B) - a_2^{\mathrm{BCS}}\cdot dn_{\mathrm{BB},i+1}^2 - a_0^{\mathrm{BCS}}}{\overline{b_{1,i+1}^{\mathrm{BB}}}}. \end{aligned} \quad (17)$$

The instantaneous correction to dn_{EV} is given by adding the linearly interpolated amount, according to

$$dn_{\mathrm{EV},i}(t) \rightarrow dn_{\mathrm{EV},i}(t) + \frac{dn_{\mathrm{EV},i}(t)}{dn_{\mathrm{BB},i}}\left(\frac{\Delta_{\mathrm{BB},i+1} - \Delta_{\mathrm{BB},i}}{2.954}\cdot t + \Delta_{\mathrm{BB},i}\right) \quad (18)$$

where the time t is measured from the center of the ith scan measurement of the OBC BB.

Generalizing (3), the radiance difference attributed to the earth view path and the space view path (after reflection by the scan mirror) is given by

$$\begin{aligned}\Delta L_{\mathrm{EV}} &= L_{\mathrm{EV\_PATH}} - L_{\mathrm{SVS\_PATH}} \\ &= \rho_{\mathrm{EV}}^{\mathrm{sm}} L_{\mathrm{EV}} + \left(\rho_{\mathrm{SV}}^{\mathrm{sm}} - \rho_{\mathrm{EV}}^{\mathrm{sm}}\right)L(T_{\mathrm{sm}}) \end{aligned} \quad (19)$$

and similarly from (8)

$$\rho_{\rm EV}^{\rm sm}\overline{L_{\rm EV}} + \left(\rho_{\rm SV}^{\rm sm} - \rho_{\rm EV}^{\rm sm}\right)\overline{L(T_{\rm sm})} = a_0^{\rm BCS}(B) + \overline{b_1^{\rm BB}(B)}\cdot dn_{\rm EV} + a_2^{\rm BCS}(B)\cdot(dn_{\rm EV})^2 \quad (20)$$

where the overstrike bar over the radiance terms (not the b_1 term) on the left-hand side of (20) indicate the appropriate RSR averaging similar to (5).

Solving (20) for the band-averaged radiance from the earth view, before the scan mirror reflection, representing the desired "at aperture" radiance $\overline{L_{\rm EV}(B)}$ yields

$$\overline{L_{\rm EV}(B)} = \frac{1}{\rho_{\rm EV}^{\rm sm}(\lambda)}\Big[a_0^{\rm BCS}(B) + \overline{b_1^{\rm BB}(B)}\cdot dn_{\rm EV} + a_2^{\rm BCS}(B)\cdot(dn_{\rm EV})^2\Big] - \frac{\rho_{\rm SV}^{\rm sm}(\lambda) - \rho_{\rm EV}^{\rm sm}(\lambda)}{\rho_{\rm EV}^{\rm sm}(\lambda)}\cdot\frac{\int L(T_{\rm sm},\lambda)\cdot{\rm RSR}(B,\lambda)\cdot d\lambda}{\int {\rm RSR}(B,\lambda)\cdot d\lambda}. \quad (21)$$

In summary, $\overline{L_{\rm EV}(B)}$ is determined by

$$\overline{L_{\rm EV}(B)} = L_{\rm EV}\big[a_0^{\rm BCS}(B), a_2^{\rm BCS}(B), \rho_{\rm SV}^{\rm sm}, \rho_{\rm EV}^{\rm sm}, \rho_{\rm BB}^{\rm sm}, \varepsilon_{\rm cav}(B), \varepsilon_{\rm BB}(B), \Delta T_{\rm BB}(B), {\rm RSR}(B,l), T_{\rm BB}, T_{\rm sm}, T_{\rm CAV}, T_{\rm inst}, {\rm DN}_{\rm EV}, {\rm DN}_{\rm BB}, {\rm DN}_{\rm SV}\big] \quad (22)$$

where the coefficients $a_0^{\rm BCS}(B)$, $a_2^{\rm BCS}(B)$, $\rho_{\rm SV}^{\rm sm}$, $\rho_{\rm EV}^{\rm sm}$, $\rho_{\rm BB}^{\rm sm}$, $\varepsilon_{\rm cav}(B)$, $\varepsilon_{\rm BB}(B)$, $\Delta T_{\rm BB}(B)$, and ${\rm RSR}(B,\lambda)$ are determined from prelaunch calibration measurements ($\Delta T_{\rm BB}(B)$ term is added to $T_{\rm BB}(B)$ from the BCS to OBC calibration transfer process) and the remaining coefficients $T_{\rm BB}$, $T_{\rm sm}$, $T_{\rm CAV}$, $T_{\rm inst}$, ${\rm DB}_{\rm EV}$, ${\rm DN}_{\rm BB}$, and ${\rm DN}_{\rm SV}$ are determined from on-orbit telemetry.

C. On-Orbit Maneuver for Scan Mirror

The MODIS scan mirror rotation produces a variable response versus scan angle (RVS) due to the 10.5–65.5° AOI variation across the 110° scan angle range, as a result of the different reflectance for s- and p-polarized light. In addition, the variable reflectance translates into a variable emission component. A system-level analytic expression of the variable RVS is complex and expected to vary with molecular contamination levels on-orbit. Attempts to measure the system-level RVS in the ambient environment were limited by the generally high-instrument photon background and the need to operate with a mechanical cooler, which lead to additional instrument noise.

To meet the MODIS radiometric uncertainty requirements, it is planned to periodically measure the response versus scan angle on-orbit. The MODIS Science Team has requested that the EOS-AM1 spacecraft be oriented to scan deep space for up to about 30 min when the spacecraft is in the earth shadow. This maneuver will provide the MODIS with a view above the horizon to observe the 3 K space background. During this orientation, the MODIS will respond to the scan angle-dependent emission from the scan mirror. The scan angle-dependent emission can then be directly related to the scan angle-dependent reflectance by Kirchhoff's law. Model estimates of the scan mirror emission signal indicate adequate SNR for the LWIR bands. The GOES-8 and -9 experiences demonstrate that these measurements can be performed to about 1% or less uncertainty for all emissive infrared bands. The GOES imager calibration for RVS is changed quarterly (Weinreb [10]). Consequently, the cold space scan maneuvers may be implemented about yearly.

IV. Reflected Solar-Band Algorithm

The two primary science data products for the reflected solar bands are the earth-exiting spectral radiance L and the earth reflectance factor $\rho\cos(\theta_{\rm Sc})$ computed for each pixel. $\theta_{\rm Sc}$ is the solar zenith angle at each pixel. Both products are extracted using the effective digital number output dn^*. The dn^* are corrected for detector dark radiance response, so that they are interpreted as signal. In producing these products, the instrument uses prelaunch calibration factors that can be verified using onboard calibrators, postlaunch special tests, and vicarious calibrations. On-orbit, the calibration factors will be changed from the prelaunch values through this verification process.

The output from the focal plane detector arrays (FPA's) are digitized, recorded, and telemetered as raw digital numbers. The instrument response for each band and detector channel (D) for an individual scene (Sc) may be written as

$$dn_{B,D}^*({\rm Sc}) = \big[{\rm DN}_{B,D}({\rm Sc})S_B({\rm MS},{\rm AOI}) - \langle {\rm DN}'_{B,D}({\rm SV})\rangle S_B({\rm MS},{\rm AOI})\big]\cdot {\rm FF}_B({\rm MS},D)\cdot\big\{1 + K_{B,D}^{\rm inst}\big[\langle T^{\rm inst}\rangle - T_{\rm Cal}^{\rm inst}\big] + K_{B,D}^{\rm FP}\big[\langle T_B^{\rm FP}\rangle - T_{{\rm Cal},B}^{\rm FP}\big]\big\}. \quad (23)$$

The analog-to-digital conversion (ADC) electronics are known to be nonlinear. The expression ${\rm DN}'$ is the telemetry output ${\rm DN}$ corrected for this ADC nonlinearity. In this expression, $S_B({\rm MS},{\rm AOI})$ is a lookup table-based correction to account for the scan mirror response variation with the mirror AOI for each scene. The two scan mirror sides are treated separately. The offset correction for the zero radiance response is made using a view of cold space from the SV through the term $\langle {\rm DN}'_{B,D}({\rm SV})\rangle$, which is computed from an average of multiple scans. The individual scenes that are used in these bands are scenes in the earth view, looking at scattering from the solar diffuser and scenes looking at the SRCA. The AOI reflectance variations in these bands are small and were adequately characterized during prelaunch calibration testing over the spectral interval 0.4–1.0 μm.

The correction for temperature variations across the FPA and electronics as well as the long-term effects of temperature variations of the instrument over the mission lifetime is applied via two linear correction terms. The average focal plane (FP) temperature $\langle T_B^{\rm FP}\rangle$ is compared with a FP reference temperature $T_{{\rm Cal},B}^{\rm FP}$, and any temperature deviations from the reference are corrected using the FP temperature coefficient $K_{B,D}^{\rm FP}$. The FP temperature coefficient is determined, for each MODIS detector, based on responsivity variations observed during thermal vacuum testing. The term $K_{B,D}^{\rm FP}[\langle T_B^{\rm FP}\rangle - T_{{\rm Cal},B}^{\rm FP}]$ is validated on-orbit using a 1-W or 10-W lamp output from the

SRCA, operated in radiometric mode over the entire orbit. A similar temperature correction for the overall instrument temperature T^{inst} is applied through the instrument temperature coefficient $K^{\text{inst}}_{B,D}$. The at-launch value of $K^{\text{FP}}_{B,D}$ is set to unity, while that of $K^{\text{inst}}_{B,D}$ is determined from ground-based thermal vacuum data.

Finally, $\text{FF}_B(\text{MS}, D)$ is a "flat fielding" or "destriping" calibration term to equalize the response of the individual detectors in a given band based on a postlaunch observation of a very low contrast scene. At launch time, this correction term is set to unity because each detector is separately calibrated, and the calibration strategy is expected to produce a product that is destriped. On-orbit, the FF_B will be validated from the observations of sunlight scattered off the onboard Spectralon solar diffuser.

The primary calibration for the radiance product at-launch is based on the laboratory calibration source. The laboratory calibration source is a 100-cm Spherical Integration Source (SIS), known as the SIS100. The SIS100 was located outside of the thermal vacuum chamber, and the sensor illumination was through a window in the chamber wall. The primary calibration for the reflectance factor product is the laboratory measurement of the solar diffuser bidirectional reflectance factor (BRF). An additional MODIS onboard calibration system is a solar diffuser stability monitor (SDSM), which operates similarly to a ratioing radiometer. This system is designed to monitor the BRF of the solar diffuser by observations of the sun directly combined with nearly simultaneous observations of the solar diffuser (SD). The SDSM is fitted with a miniature spherical integration sphere and nine silicon photodiodes. The nine SDSM bands monitor the SD BRF between 0.42 and 0.95 μm. The reflectance factor calibration values will be adjusted during the mission based on measurements from the SDSM.

A. Radiance Product

The EV band spectral radiance is obtained by an integration over a band and is given by

$$L_{B,D}(\text{EV}) = \frac{\int_{\lambda_1}^{\lambda_2} L_\lambda(\text{EV}) \cdot \text{RSR}_{\lambda,B,D} d\lambda}{\int_{\lambda_1}^{\lambda_2} \text{RSR}_{\lambda,B,D} d\lambda} \tag{24}$$

where $L_\lambda(\text{EV})$ is the spectral radiance of the earth scene at wavelength λ, $\text{RSR}_{\lambda,B,D}$ is the relative spectral response at wavelength λ, normalized to unity at the peak response, and λ_1 and λ_2 are the wavelength range over which the detector has a significant quantum efficiency.

The prelaunch responsivity $\Re^*_{\text{Cal},L,B,D}$ is defined by

$$\Re^*_{\text{Cal},L,B,D} = \frac{dn^*_{\text{Cal},B,D}(\text{SIS100})}{L_{\text{Cal},B,D}(\text{SIS100}) - L^0_{\text{Cal},L,B,D}}. \tag{25}$$

In the above expression, L^0 denotes an offset that may be needed to account for any deviations from zero radiance during calibration. The uncertainty of the calibration of the SIS100, given in (25) by $L_{\text{Cal},B,D}(\text{SIS100})$, is validated through EOS SIS comparisons [11].

The time-dependent radiance responsivity $\Re^*_{L,B,D}(t)$ is the radiance calibration factor for the MODIS at the time t. We construct $\Re^*_{L,B,D}(t)$ as a product of the prelaunch value with the change on transfer to orbit as determined at the first use of the solar diffuser and the change in orbit after the first use of the SD.

$$\Re^*_{L,B,D}(t) = \Re^*_{\text{Cal},L,B,D}(\text{SIS} - 100) \cdot (\alpha_{B,D} \exp(-\gamma_{B,D} t) + \beta_{B,D} t). \tag{26}$$

At launch, α is preset to unity, while β and γ are preset to zero for all detectors. These quantities are checked on orbit during initial sensor operations by comparing the response of the MODIS to the SRCA operated in the radiance mode during the on-orbit calibration, with the response obtained during the ground calibration in a comparable operating mode; they also will be checked periodically during the mission. The zero radiance offset L^0_{Cal} of (25) also may have a time variation in a similar manner as (26).

The radiance product can be checked on-orbit also by comparison of the multiplicative result

$$\Re^*_{\text{Cal},L,B,D}(\text{SIS} - 100) \cdot \alpha_{B,D} \tag{27}$$

with vicarious calibration measurements during the validation phase of the program as well as with the reflectance product in conjunction with a standard solar spectral irradiance [12]. Note that the best use of ground-truth vicarious calibration in this formulation is to check or correct the calibration scale at the first use of the SD, as shown in (27).

The final calibration expression is

$$L_{B,D}(\text{EV}) = L^0 + \frac{dn^*_{B,D}(\text{EV})}{\Re^*_{L,B,D}}. \tag{28}$$

B. Reflectance Product

In addition to its function as a radiometer, operating in the earth view radiance mode, the MODIS will be used on orbit as a reflectometer. In this mode, the MODIS will act as a transfer radiometer between two diffuse reflecting surfaces, the SD and the earth. The SD and the earth atmosphere system are reflecting surfaces with a common illuminating source, the sun.

When viewing the earth, the earth-atmosphere BRF $\rho_{\text{EV},B,D}$ is extracted from the EV radiance and the solar irradiance $E_{\text{SUN},B,D}$ for any detector of a given band by

$$\rho_{\text{EV},B,D} = \frac{\pi L_{B,D}(\text{EV})}{E_{\text{SUN},B,D} \cos(\theta_{\text{EV}})} \tag{29}$$

where θ_{EV} is the solar zenith angle for that pixel or that scene. A comparison of the BRF of the earth to the BRF of the SD $\rho_{\text{SD},B,D}$, which is defined in a similar fashion as the above equation, gives the reflectance data product of MODIS, namely

$$\begin{aligned} \rho_{\text{EV},B,D} \cos(\theta_{\text{EV}}) &= \frac{L_{B,D}(\text{EV})}{L_{B,D}(\text{SD})} \rho_{\text{SD},B,D} \cos(\theta_{\text{SD}}) \\ &= \frac{L_{B,D}(\text{EV})}{L_{B,D}(\text{SD})} \frac{\text{BRF}_B(\theta_{\text{SD}})}{\pi} \end{aligned} \tag{30}$$

where θ_{SD} is the angle of the sun on the SD. The $\cos(\theta_{\mathrm{SD}})$ term is included in (30) because the sun direction to SD is not normal to the SD. The uncertainty of the calibration of the SD, given in (30) by $\rho_{\mathrm{SD},B,D}$, is validated through EOS diffuse reflectance standards comparisons [11].

This formulation works well in the instance that the BRF of the SD is flat across the sensor bandpass. For the Spectralon diffuser, this is achieved in all of the MODIS reflected solar bands, although there is a small error in Band 7 due to the diffuser reflectance feature at 2.15 μm [13]. The ratio of the band-integrated spectral radiances $\frac{L_{B,D}(\mathrm{EV})}{L_{B,D}(\mathrm{SD})}$ in the above equation shows the use of MODIS as a ratioing radiometer with the solar diffuser as the reference sample. The above equation can be cast in a form that shows the direct relation to the measured effective digital numbers using the calibration (28) (assuming that the zero radiance term L^0 is negligible)

$$\rho_{\mathrm{EV},B,D}\cdot\cos(\theta_{\mathrm{EV}}) = \frac{dn^*_{B,D}(\mathrm{EV})}{dn^*_{B,D}(\mathrm{SD})}\rho_{\mathrm{SD},B,D}(t_{\mathrm{SD}})\cdot\cos(\theta_{\mathrm{SD}}). \tag{31}$$

The SD/SDSM time series will be used on-orbit to track changes in $\rho_{\mathrm{SD},B,D}$ over time; since the measurement of $dn^*_{B,D}(\mathrm{SD})$ may occur as much as a week earlier than the measurement of $dn^*_{B,D}(\mathrm{EV})$, $dn^*_{B,D}(\mathrm{SD})$ may need to be adjusted to account for changes in the earth–sun distance over the time frame between two measurements. The schedule for repeated solar measurements of the SD will be set so that changes in the BRF of the SD are small (compared to a 2% calibration uncertainty requirement) between successive observations.

The prelaunch laboratory characterization of the SD determines its reflectance properties. No system-level prelaunch calibration of the SD/SDSM exists. There is no method to monitor changes in this characterization from the laboratory to orbit. The analysis of $\rho_{\mathrm{SD},B,D}(t_{\mathrm{SD}})$ from (30) is analogous to that shown for (26)

$$\rho_{\mathrm{SD},B,D}(t_{\mathrm{SD}}) = \rho_{\mathrm{SD,Cal},B,D}(\alpha_{B,D}\exp(-\gamma_{B,D}t) + \beta_{B,D}t). \tag{32}$$

Again, α is set to one, while β and γ are set to zero; the term $\rho_{\mathrm{SD,Cal},B,D}\alpha_{B,D}$ can be compared to available ground-truth measurements.

V. L1B Data Product Description

The MODIS Level 1B software data product contains the radiometrically corrected and fully calibrated instrument data in physical units at the original instrument spatial and temporal resolution.

These data are broken into granules approximately 5-min long and stored in hierarchical data format (HDF), separated into the following four files:

1) **MODIS Level 1B 250 M Earth View Data Product**, which contains earth view observations in scientific units for the MODIS Bands 1 and 2 at 250-m spatial resolution;
2) **MODIS Level 1B 500 M Earth View Data Product**, which contains earth view observations in scientific units from the MODIS Bands 1 and 2, aggregated at 500-m spatial resolution, plus the earth view observations from MODIS Bands 3 through 7 at 500-m spatial resolution;
3) **MODIS Level 1B 1 KM Earth View Data Product**, which contains earth view observations in scientific units from the MODIS Bands 1 through 7, aggregated at 1-km spatial resolution, plus the earth view observations from MODIS Bands 8 through 36 at 1-km spatial resolution;
4) **MODIS Level 1B OBC/E Product**, which contains OBC observations in raw DN's from all MODIS bands at their original resolution, plus the engineering data in engineering units.

The aggregation algorithm used in the 500-m and 1000-m earth view files is documented at [13].

Fig. 4 shows the different components of the Level 1B HDF files. The product contains five types of metadata, which describe the data components, their contents, and their attributes. These are core metadata, archive metadata, product metadata, swath metadata, and scientific data sets (SDS) metadata. The core, archive, and product metadata are stored once in each file as HDF global attributes. The swath metadata, stored for each complete scan (one side of the scan mirror), are in two forms: swath attributes for HDF-EOS required swath metadata and HDF Vdata for Level 1B specific swath metadata. Vdata are tables of fixed field length, as in a vector format. The SDS metadata are stored as SDS attributes and do not explicitly appear in the figure. The various types of metadata are used for different purposes within the production and archive environment. Some are stored in a searchable database for product tracking and queries by science users. The remainder serve as easily accessible descriptive and summary information.

The science data in the earth view files are instrument data and geolocation data stored as multiple SDS's in HDF-EOS swath format. A small subset of internal geolocation data are stored in the MODIS 1 KM Earth View Data Product for convenience in imaging and visualization. The idiosyncrasies of the way the science data are stored are captured by the self-describing capabilities of HDF.

The corrected raw counts dn^* from the instrument are stored as 15-bit integers in the software L1B data product for the reflected solar bands. The radiance (reflectance factor) product for each band in the reflected solar bands is computed as

$$L_{B,D} = g0_{B,D} + g1_{B,D}\cdot dn^*. \tag{33}$$

A linear calibration equation is used for these bands, as the $g1_{B,D}$ corresponds to the $1/\Re^*_{L,B,D}$ from (25) and $g0_{B,D}$ term is a residual term from the fitting of the $g1_{B,D}$ for the calibration data sets and corresponds with L^0. The g coefficients are included in the granule-level metadata.

A similar approach to (33) is used for the thermal emissive bands, except $\hat{dn}$ is stored as the 15-bit integer. The $\hat{dn}$ is an integer that produces the radiance for these bands

$$L_B = g0_B + g1_B\cdot\hat{dn}. \tag{34}$$

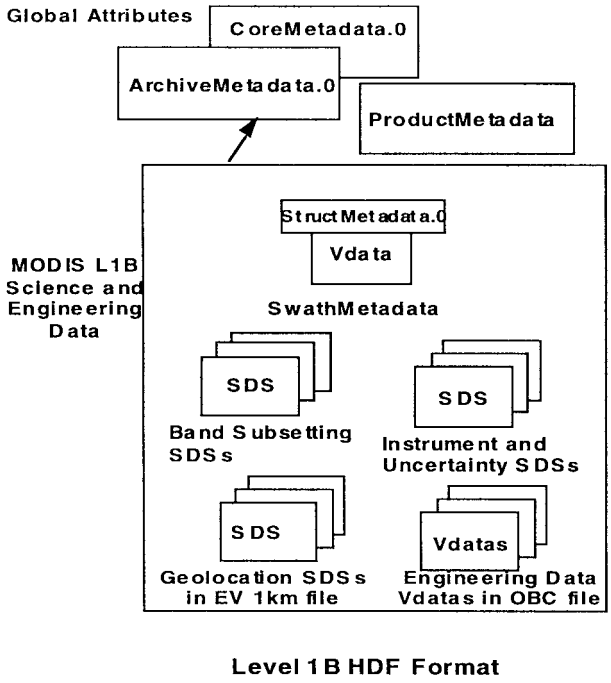

Fig. 4. MODIS Level 1B HDF format is depicted. The five types of metadata are identified, and the types of Vdata and SDS files are identified.

In (34), $\hat{dn}$ is not related to dn^*. The dn^* cannot be used for the thermal emissive bands because the calibration for (22) is not a linear calibration. The $g0_B$ and $g1_B$ terms are scaling terms for the thermal emissive bands and are computed for each granule and provided in the granule-level metadata. The calibration coefficients for the thermal emissive bands are embedded in the g coefficients in the metadata. This approach is chosen to conserve output file space.

Invalid data fields are identified by having the highest order bit set to one. The datum in a field is marked as invalid for the following reasons:

1) flagged as missing from the Level 1A data set;
2) detector is dead;
3) value is saturated;
4) calibration failure.

Thus, any datum larger than 32 767 should be interpreted as invalid. The values in data fields that are flagged as missing from the Level 1A data set are equal to 65 535, regarded as unsigned 16-bit integers. For invalid data not flagged as missing from the Level 1A data set, the actual values stored in the file are the corrected raw counts calculated by the algorithm, stored as 15-bit unsigned integers, with the high-order bit of the 16-bit word set to one.

Associated with each instrument data value is uncertainty information about that value. The information is reported in an 8-bit word, with the four most significant bits used for an uncertainty index and the other four bits used for a scene contrast index. The scene contrast index is not implemented at this time. Uncertainty information is reported as an index to conserve output file space. The uncertainty index is carried as a multiplicative factor to be applied to the instrument spectral radiance specifications provided below. The index translates to an uncertainty value by use of the formula

$$0.5 * \exp(\text{Uncertainty Index}/N) = \pm\text{Uncertainty Range Multiplier Value}. \quad (35)$$

The uncertainty is identified as a one-sigma uncertainty. The specific uncertainty range for any band is obtained as the product of (the uncertainty range multiplier value) $*$ (the specification uncertainty). The value of N for the thermal emissive bands is five, and the value of N for the reflected solar bands is nine. An uncertainty index value of 15 indicates that the uncertainty has not been computed. An uncertainty index value of 14 indicates that the data for this pixel are contaminated by an electronic nonlinearity and not properly calibrated.

The specification for uncertainty in the reflected solar bands for the reflectance factor product is $\pm 2\%$ for all bands, all detectors. The specification in the reflected solar bands for the radiance product is $\pm 5\%$ for all bands, all detectors. The specification for the radiance calibration uncertainty in the thermal emissive bands is $\pm 1\%$ for all bands, all detectors, except for Band 20, which is $\pm 75\%$ and Bands 31 and 32, which is $\pm 0.5\%$.

VI. Concluding Comments and Summary

The material describing the at-launch MODIS radiometric product has been presented without a discussion of the actual polarization in the reflected solar bands. The specification for these bands is that the residual polarization sensitivity is not greater than 0.02 for bands with a center wavelength between 0.43 and 2.2 μm for the principal scan angles between $+45°$ and $-45°$. This performance specification is satisfied for most instances. Nevertheless, variations among detectors in some bands may impact the flat-fielding determination described in (23). Data from bands 1–19 are available only when the sensor is operated in the "day mode." Band 26 data are available in both day mode and night mode operations.

The MODIS principle radiometric products in the emissive infrared bands are radiance. The MODIS principle radiometric products in the reflected solar bands are radiance and reflectance factor. In all three instances, an at-launch calibration equation is summarized. The traceability of the calibration standard is presented. The techniques to verify the at-launch calibration throughout the mission lifetime are presented. The MODIS data user is encouraged to use the MCST homepage on the World Wide Web for current calibration and characterization parameters.

References

[1] W. L. Barnes, T. S. Pagano, and V. V. Salomonson, "Prelaunch characteristics of the Moderate Resolution Imaging Spectroradiometer (MODIS) on EOS-AM1," this issue, pp. 1088–1100.
[2] W. E. Esaias, M. R. Abbott, O. W. Brown, J. W. Campbell, K. L. Carder, D. K. Clark, R. L. Evans, F. E. Hoge, H. R. Gordon, W. P. Balch, R. Letelier, and P. Minnett, "An overview of MODIS capabilities for ocean science observations," this issue, pp. 1250–1265.
[3] C. O. Justice, E. Vermote, J. R. G. Townshend, R. Defries, D. P. Roy, D. K. Hall, V. V. Salomonson, J. L. Privette, G. Riggs, A. Strahler, W. Lucht, R. B. Myneni, Y. Knyazikhin, S. W. Running, R. R. Nemani, Z. Wan, A. R. Huete, W. van Leeuwen, R. E. Wolfe, L. Giglio, J.-P. Muller, P. Lewis, and M. J. Barnsley "The Moderate Resolution

Imaging Spectroradiometer (MODIS): Land remote sensing for global change research," this issue, pp. 1228–1249.
[4] Labsphere Corporation, *A Guide to Reflectance Materials and Coatings*, North Sutton, NH, 1996, p. 3.
[5] J. Young, "PFM MWIR/LWIR radiometric calibration I: Theory and measurement equations," Raytheon Santa Barbara Remote Sensing, Goleta, CA, SBRS Memo. PL3095-N06555, 1997.
[6] D. Knowles, M. Jones, H. Montgomery, and L. L. Goldberg, "Algorithm theoretical basis document 1996 thermal calibration algorithm," NASA's Goddard Space Flight Center, Greenbelt, MD, MCST Ref. G031, 1996, p. 48.
[7] G. Godden, S.-Y. Qiu, and X. Xiong, "The MODIS polarized radiance calibration algorithm," NASA's Goddard Space Flight Center, Greenbelt, MD, MCST Memo., Apr. 1998.
[8] M. Cafferty, private communication, 1995.
[9] M. E. MacDonald, "Testing of mirror as a function of wavelength and polarization at varying angles of incidence," Mass. Inst. Technol. Lincoln Lab., Lexington, Sept. 26, 1997.
[10] M. Weinreb, M. Jamieson, N. Fulton, Y. Chen, J. X. Johnson, C. Smith, J. Bremmer, and J. Baucom, "Operational calibration of the imagers and sounders on the GOES-8 and -9 satellites," NOAA, Washington, DC, NOAA Tech. Memo. NESDIS 44, Feb. 1997.
[11] J. J. Butler and R. A. Barnes, "The calibration strategy for the Earth Observing System (EOS)-AM1 platform," this issue, pp. 1056–1061.
[12] G. Thuillier, M. Herse, P. C. Simon, D. Labs, H. Mandel, and D. Gillotay, "Observations of the solar spectral irradiance from 200 to 850 nm during the ATLAS missions by the SOLSPEC spectrometer," presented at *New Developments and Applications in Optical Radiometry (NEWRAD'97)*, Opt. Sci. Center, Univ. Arizona, Tucson, Oct. 1997, pp. 27–29.
[13] B. Guenther, "Ground calibration and in-orbit use of diffusers for earth observations using MODIS as an example," presented at *New Developments and Applications in Optical Radiometry (NEWRAD'97)*, Opt. Sci. Center, Univ. Arizona, Tucson, Oct. 1997, pp. 27–29.
[14] M. Nishihama, R. Wolfe, D. Salomonson, F. Patt, J. Blanchette, E. Masuoka, and A. Fleig, "MODIS level 1A earth location," *Algorithm Theoretical Basis Document*, version 3.0, NASA's Goddard Space Flight Center, Greenbelt, MD, SDST Ref. 092, 1997.

B. Guenther, photograph and biography not available at the time of publication.

Gerald D. Godden, photograph and biography not available at the time of publication.

Xiaoxiong Xiong, photograph and biography not available at the time of publication.

Edward J. Knight, photograph and biography not available at the time of publication.

Shi-Yue Qiu, photograph and biography not available at the time of publication.

Harry Montgomery, photograph and biography not available at the time of publication.

M. M. Hopkins, photograph and biography not available at the time of publication.

Mohammad G. Khayat, photograph and biography not available at the time of publication.

Zhidong Hao, photograph and biography not available at the time of publication.